J. Fluid Mech. (1984), *vol.* 142, *pp.* 363–381
Printed in Great Britain

Natural convection in an inclined square cavity in regions of density inversion of water

By HIDEO INABA AND TAKEYUKI FUKUDA
Department of Mechanical Engineering, Katami Institute of Technology,
Koen-Cho 165, Kitami, Hokkaido 090, Japan

(Received 15 August 1983)

The steady laminar natural convection of water in an inclined square cavity is investigated experimentally and analytically at temperatures in the neighbourhood of maximum density near 4 °C. One hot wall of the square cavity is maintained at various uniform temperatures from 2 to 20 °C and the opposing cold wall is kept at a uniform temperature of 0 °C, while the other walls are thermally insulated. Photographs and analytical descriptions of the flow patterns, temperature profiles in the water layer and average heat-transfer coefficients are presented in this paper for various surface temperatures T_h of the hot wall and inclination angles of the square cavity θ from 0° (heated from below) to 180° (heated from above) by 30° intervals. From this study it should be noted that the density inversion of water has a strong effect on the natural convection occurring in the inclined square cavity, and the average heat-transfer coefficient is a peculiar function of the surface temperature of the hot wall, unlike previous results for Boussinesq fluids without density inversion. Solutions of the governing equations for steady two-dimensional laminar natural convection are obtained numerically, and the results obtained agree reasonably well with the experimental ones in the ranges of $30^c < \theta \leqslant 180°$ for $T_h > 8$ °C, $0° \leqslant \theta \leqslant 120°$ for $T_h < 8$ °C, and $0° \leqslant \theta \leqslant 180°$ for $T_h = 8$ °C.

1. Introduction

It is well known that the natural convection occurring from temperature variation of water in the neighbourhood of the ice–water interface has an important role in the formation of ice on a lake or river and the freezing of water pipes, water-storage vessels or fire hydrants in cold regions. An ice–water interface such as in these examples is commonly inclined, since rarely is the Earth's surface aligned with geopotential lines. This paper reports a study of the steady natural convection of water in the neighbourhood of maximum density near 4 °C in an inclined square cavity. Many studies on natural convection in an inclined rectangular cavity filled with a Boussinesq fluid (a monotonic relation between density and temperature) have previously been performed. It seems that Degraaf & Van Der Held (1953) were the first to consider the titled convection problem. Hart (1971) performed a series of flow-visualization experiments for various inclination angles to examine flow instability in the water layer. He observed the existence of longitudinal rolls with axes directed up slope, roll-dominated turbulence and transverse travelling waves depending on inclination angles θ and temperature differences between surface temperatures of the hot and cold walls. Ozoe, Sayama & Churchill (1977) reported similar flow behaviours and measurements of heat-transfer rate for aspect ratio H/W (height to width of the rectangular cavity) = 1–15.5 in air as well as higher-Prandtl-number fluid. Clever & Busse (1977) investigated the stability of longitudinal rolls in an

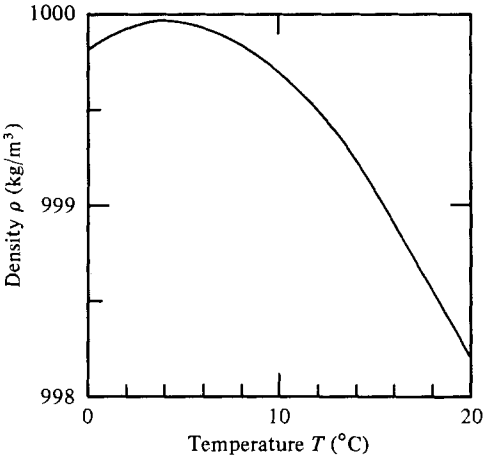

FIGURE 1. Relationship between density and temperature for water near 4 °C.

inclined convection layer. They reported three types of flow instabilities which were responsible for the transition from longitudinal rolls to three-dimensional flows of natural convection. Ruth, Rathby & Hollands (1980) observed the secondary transition in the convective motion in the region $\theta > 20°$. Linthorst, Schinkel & Hoogenoorn (1981) determined experimentally the transition from stationary to non-stationary flow and the transition from two-dimensional to three-dimensional flow.

However, for natural convection of water in the neighbourhood of the ice–water interface, it seems that peculiar flow behaviour, which could not be seen in a Boussinesq fluid, appears in the water layer since its density has the maximum value near 4 °C, with zero coefficient of cubical expansion, as can be seen in figure 1. Studies of natural convection in a melting horizontal layer of ice heated from below or above have been reported by Tien (1968), Yen & Gale (1969), Sun, Tien & Yen (1969), Sugawara, Fukusako & Seki (1974) and Merker & Straub (1982). On the other hand, Watson (1972) and Seki, Fukusako & Inaba (1978) investigated analytically and experimentally the natural convection of water involving the density-inversion region in a confined rectangular cavity, in which one vertical wall was kept at the freezing temperature of water and the opposing vertical wall was maintained at various temperatures above the freezing temperature. They reported that there appeared two counter-rotating steady eddies in the cavity, and that the average heat-transfer coefficient was a function of temperature difference between surface temperatures of opposing vertical hot and cold (0 °C) walls. Furthermore they mentioned that the heat-transfer coefficient had a minimum value at the surface temperature of the hot wall $T_h = 8$ °C, where two counter-rotating eddies of almost the same size coexisted in the cavity. But little attention has been paid to date to obtaining information about natural convection in the inclined rectangular cavity with density inversion of water, which is important in predicting the formation or decay of an inclined ice layer.

The primary objective of this study is to obtain fundamental information about the effect of density inversion of water near 4 °C on natural convection flow patterns and heat-transfer rates in an inclined square cavity, whose two opposing wall-surface temperatures are maintained isothermally (but differentially). That is, the surface temperature of the cold wall T_c is maintained at 0 °C, while that of the opposing hot

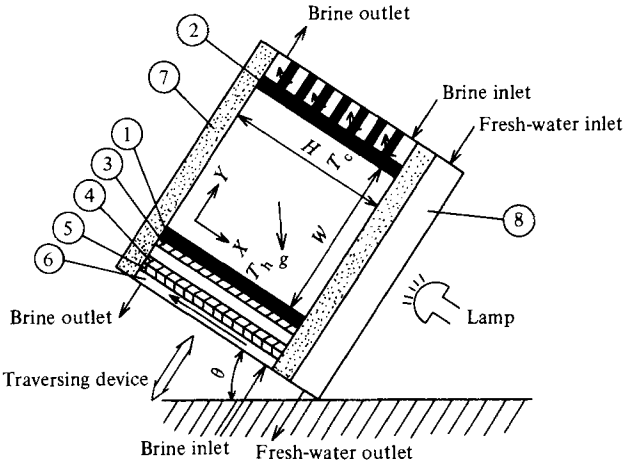

FIGURE 2. Schematic diagram of the experimental apparatus: ① heating wall (T_h); ② cooling wall (0 °C); ③ main heater; ④ guard heater; ⑤ aluminium plate; ⑥ cooling chamber; ⑦ insulating material; ⑧ filter for radiation.

wall T_h is varied from 2 to 20 °C. The inclination angle θ of the square cavity is changed from $\theta = 0°$ (heated from below) to $\theta = 180°$ (heated from above) by 30° intervals. The present results refer to visual flow patterns, temperature profiles in the water layer and average Nusselt number $Nu = qW/\lambda\,\Delta T$, where W is the width of the cavity, λ is the heat conductivity, ΔT is the temperature difference between the hot and cold walls, and q is the heat transferred per unit area and time. In addition some experimental results obtained are compared with the numerical ones based on steady two-dimensional laminar natural convection with density inversion of water in an inclined square cavity by solving the governing equations, which readily admit variation of the physical properties of the fluid with temperature.

2. Description of experimental apparatus and procedure

The present experiments were carried out using an inclined water-filled rectangular cavity with one wall kept at 0 °C and the opposing wall maintained at various temperatures above 0 °C. The main parts of the experimental apparatus consisted of a heating part, a water-filled test section and a cooling part as depicted in figure 2. The test section was constructed by inserting a lucite frame (10 mm thickness) of 15 mm (height H) × 15 mm (width W) sectional area and depth $D = 100$ mm between the heating and cooling parts. The inner surfaces of the test section were painted black in order to avoid reflection of the light beam for visual observations, except for a slit for the light beam and a front wall made of lucite plate for the convenience of the visual observation of flow patterns.

The surface temperature of the cold wall (copper plate of 5 mm thickness) was uniformly kept at 0 °C by inducing a temperature-controlled coolant into the cooling chamber attached to the outside of the cold wall. The surface temperature of the hot wall (copper plate of 5 mm thickness) was uniformly maintained at a constant temperature above 0 °C using a controllable main mica electrical heater which was mounted on the rear side of the main heater across a Bakelite plate (5 mm thickness) to minimize the heat loss from the main heater to the environment. The other cooling

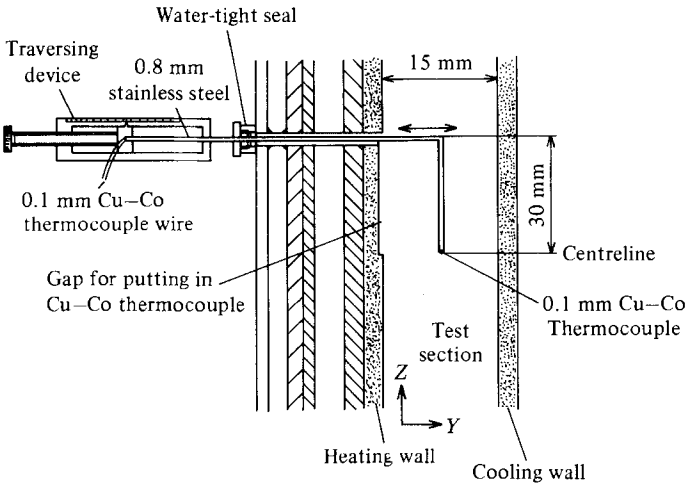

FIGURE 3. Physical model of an inclined square cavity.

chamber was equipped on the rear side of the guard heater to absorb the heat from the guard heater. It was possible to control the surface temperature gradients of the hot wall and cold wall in the X-direction to within ± 0.1 °C/cm. The temperature gradients of the hot and cold walls were evaluated from the temperature measurements with Cu–Co thermocouples (0.1 mm in diameter) embedded into the copper plates of the hot and cold walls at positions $X^* = 0.1$, 0.5 and 0.9 and at the halfway position ($Z = 50$ mm) in the depth direction ($D = 100$ mm). One small probe (a stainless-steel pipe of 0.8 mm diameter) having a Cu–Co thermocouple of 0.1 mm in diameter was arranged at the position $X = \frac{1}{2}H$ ($X^* = 0.5$) in order to measure the temperature distribution in the water layer in the Y-direction. The probe was traversed from the hot wall to the cold wall by a traversing device, which was composed of a micrometer mechanism, a guide pipe (1 mm inside diameter) set into the heating part, and a moving stainless-steel pipe (0.8 mm diameter) with thermocouple, as can be seen in figure 3. The temperature measurements on the test section, after the visual observation of flow patterns and measurements of heat flow, were carried out by moving the traversing device very slowly and then keeping it still over a 3–5 min period at the given measuring position. From the results of visual observations of flow patterns, it could be seen that the probe in the test section hardly disturbed the flow field, owing to the very slow circulation rate of the convective flows in the present study, in spite of the small test section.

In order to minimize the heat loss from the experimental apparatus, it was covered with Styrofoam insulating material of 100 mm thickness, except during the visual observation, and was placed in a temperature-controllable cold room, which was maintained at the average of the surface temperatures of the hot and cold walls. The heat loss in the present temperature range of $T_h = 2$–20 °C was ascertained to be less than $\pm 6\%$ from the results of the preliminary experiments, which were performed by packing ethylene glycol of thermal conductivity $\lambda = 0.24$ W/mK at 0 °C into the test section at the inclination angle $\theta = 180°$ (heated from above) without the existence of natural convection.

To visualize the flow patterns, a 100 W projection lamp was arranged under the test section as seen in figure 2. The radiant energy of the light beam was eliminated by passing cold water through a jacket of 20 mm thickness. The tracer particles were

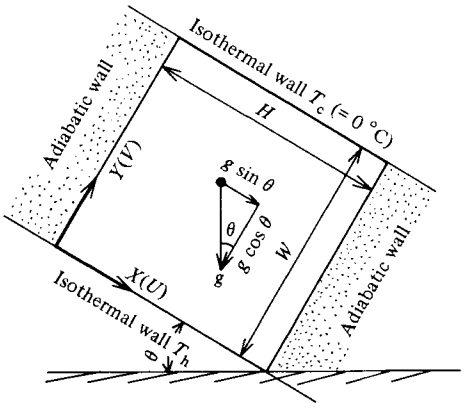

FIGURE 4. Detail of traversing device for temperature measurement of water.

a mixture of aluminium powder and white detergent or detergent only. The aluminium tracer particles of small equivalent diameter (5–10 μm) were mingled in the distilled water containing the alcohol and detergent in order to obtain a good affinity between the tracer particles and test fluid (water). After they were clarified in the container for about 24 h, the aluminium tracer particles floating in a middle layer in the container were decanted by a syringe. These tracer particles were maintained at the average temperature of the hot and cold walls for 5–10 min. They were injected slowly into the test section from the syringe. Therefore it could be said that the tracer particles used in the present study were neutrally buoyant to the test fluid.

Distilled water was used as a testing fluid to avoid the mixing of undesirable air bubbles. Photographs of the flow patterns were taken by using ASA 400 film. Typical exposure times were varied from 15 to 60 s. The experimental data were taken after the thermal and fluid-dynamic conditions had reached a steady state. It took about 6–15 h to reach the steady state. The temperature of the hot wall was varied every 2 °C ranging from 2 to 20 °C. The inclination angle θ was increased from 0° to 180° by 30°.

3. Description of numerical analysis

In this section we seek a mathematical description of the steady two-dimensional (X, Y) and laminar flow in an inclined square cavity whose one hot wall is maintained at various uniform temperature, and the opposing cold wall is kept at 0 °C, while the other walls are thermally insulated, as depicted in figure 4. The studies of Watson (1972) and Seki *et al.* (1978) on natural convection under the influence of density inversion of water in a rectangular cavity suggested that the effect on the flow field and convective heat transfer of variations of physical properties such as viscosity or thermal conductivity could not be neglected. The governing equations expressing conservation of mass, momentum and energy are formulated in a manner which admits the variation of all physical properties of water with temperature, and these values are approximated as a function of temperature by polynomials of 4th or 5th degree. For example, the non-dimensional density–temperature relationship is approximated as the followng form:

$$\rho^* = (1 + aT + bT^2 + cT^3 + dT^4)^{-1}, \tag{1}$$

where

$$a = -0.678964520 \times 10^{-4}\ ^\circ\mathrm{C}^{-1}, \quad b = 0.907294338 \times 10^{-5}\ ^\circ\mathrm{C}^{-2},$$

$$c = -0.964568125 \times 10^{-7}\ ^\circ\mathrm{C}^{-3} \quad \text{and} \quad d = 0.873702983 \times 10^{-9}\ ^\circ\mathrm{C}^{-4}.$$

Referring to the coordinate system of the inclined square cavity as shown in figure 4, the usual vorticity component ω is introduced:

$$\omega = \frac{\partial V}{\partial X} - \frac{\partial U}{\partial Y}. \tag{2}$$

The velocities U and V in the X- and Y-directions respectively are then expressed in terms of the stream function ψ by using the following relations:

$$U = \frac{\rho_c}{\rho}\frac{\partial \psi}{\partial Y}, \quad V = -\frac{\rho_c}{\rho}\frac{\partial \psi}{\partial X}. \tag{3}$$

where subscript c means the value for water at 0 °C.

We introduce the following non-dimensional variables into the governing equations:

$$\left.\begin{gathered} X^* = \frac{X}{W}, \quad Y^* = \frac{Y}{W}, \quad U^* = \frac{UW}{\nu_c}, \quad V^* = \frac{VW}{\nu_c}, \\ \Omega = \frac{\omega W^2}{\nu_c}, \quad \Psi = \frac{\psi}{\nu_c}, \quad \rho^* = \frac{\rho}{\rho_c}, \quad \mu^* = \frac{\mu}{\mu_c}, \quad T^* = \frac{T - T_c}{T_h - T_c}, \quad c_p^* = \frac{c_p}{c_{pc}}, \\ \lambda^* = \frac{\lambda}{\lambda_c}, \quad Pr_c = \frac{\mu_c c_{pc}}{\lambda_c}, \quad Gr_c^* = \frac{gW^3}{\nu_c^2}, \end{gathered}\right\} \tag{4}$$

where ν is the kinetic viscosity, μ the viscosity, c_p the specific heat, λ the thermal conductivity, Pr_c the Prandtl number and Gr_c^* the Grashof number. Then the non-dimensional equations of conservation of mass, momentum and energy may be written as follows:

$$-\frac{\partial}{\partial X^*}\left(\frac{1}{\rho^*}\frac{\partial \Psi}{\partial X^*}\right) - \frac{\partial}{\partial Y^*}\left(\frac{1}{\rho^*}\frac{\partial \Psi}{\partial Y^*}\right) - \Omega = 0, \tag{5}$$

$$\frac{\partial}{\partial X^*}\left(\Omega\frac{\partial \Psi}{\partial Y^*}\right) - \frac{\partial}{\partial Y^*}\left(\Omega\frac{\partial \Psi}{\partial X^*}\right) - \frac{\partial}{\partial X^*}\left(\frac{\mu^*}{(Gr_c^*)^{\frac{1}{2}}}\frac{\partial \Omega}{\partial X^*}\right) - \frac{\partial}{\partial Y^*}\left(\frac{\mu^*}{(Gr_c^*)^{\frac{1}{2}}}\frac{\partial \Omega}{\partial Y^*}\right)$$
$$+ \frac{\partial \rho^*}{\partial Y^*}\sin\theta + \frac{\partial \rho^*}{\partial X^*}\cos\theta + A^* = 0, \tag{6}$$

where

$$A^* = \frac{\partial \rho^*}{\partial X^*}\left(U^*\frac{\partial U^*}{\partial Y^*} + V^*\frac{\partial V^*}{\partial Y^*}\right) - \frac{\partial \rho^*}{\partial Y^*}\left(U^*\frac{\partial U^*}{\partial X^*} + V^*\frac{\partial V^*}{\partial X^*}\right) - \left(\frac{\partial^2(\mu^*/(Gr_c^*)^{\frac{1}{2}})}{\partial X^{*2}}\right.$$
$$\left. - \frac{\partial^2(\mu^*/(Gr_c^*)^{\frac{1}{2}})}{\partial Y^{*2}}\right)\left(\frac{\partial U^*}{\partial Y^*} + \frac{\partial V^*}{\partial X^*}\right) - 2\frac{\partial^2(\mu^*(Gr_c^*)^{\frac{1}{2}})}{\partial X^*\partial Y^*}\left(\frac{\partial V^*}{\partial Y^*} - \frac{\partial U^*}{\partial X^*}\right) - \frac{\partial(\mu^*/(Gr_c^*)^{\frac{1}{2}})}{\partial X^*}$$
$$\times\left(\frac{\partial^2 U^*}{\partial X^*\partial Y^*} + \frac{\partial^2 V^*}{\partial X^{*2}} + 2\frac{\partial^2 V^*}{\partial Y^{*2}}\right) - \frac{\partial(\mu^*/(Gr_c^*)^{\frac{1}{2}})}{\partial Y^*}\left(\frac{\partial^2 V^*}{\partial X^*\partial Y^*} + 2\frac{\partial^2 U^*}{\partial X^{*2}} + \frac{\partial^2 U^*}{\partial Y^{*2}}\right),$$

$$Pr_c\, c_p^*\left(\frac{\partial}{\partial X^*}\left(T^*\frac{\partial \Psi}{\partial Y^*}\right) - \frac{\partial}{\partial Y^*}\left(T^*\frac{\partial \Psi}{\partial X^*}\right)\right) - \frac{\partial}{\partial X^*}\left(\frac{\lambda^*}{(Gr_c^*)^{\frac{1}{2}}}\frac{\partial T^*}{\partial X^*}\right) - \frac{\partial}{\partial Y^*}\left(\frac{\lambda^*}{(Gr_c^*)^{\frac{1}{2}}}\frac{\partial T^*}{\partial Y^*}\right) = 0. \tag{7}$$

The vanishing of the velocity as well as the uniformity of surface temperatures on the hot ($Y^* = 0$) and cold ($Y^* = 1$) walls requires the following boundary conditions:

$$\frac{\partial \Psi}{\partial X^*} = \frac{\partial \Psi}{\partial Y^*} = 0, \quad T^* = 1 \quad (Y^* = 0), \tag{8}$$

$$\frac{\partial \Psi}{\partial X^*} = \frac{\partial \Psi}{\partial Y^*} = 0, \quad T^* = 0 \quad (Y^* = 1). \tag{9}$$

Assuming that the rigid boundary surfaces $X^* = 0$ and 1 ($H = W$) are thermally insulated, we obtain the following boundary conditions:

$$\frac{\partial \Psi}{\partial Y^*} = \frac{\partial \Psi}{\partial X^*} = 0, \quad \frac{\partial T^*}{\partial X^*} = 0 \quad (X^* = 0, 1). \tag{10}$$

In view of the mathematical complexity involved in solving the (5) – (10), a numerical computation is performed using the upwind-difference method. The number of gridpoints in the X^* and Y^* directions is 21. This number of gridpoints is employed to ensure the desired accuracy of the numerical results after each grid size is extensively examined to obtain the convergence of the flow and heat-transfer results. In the iterative procedure used to solve the abovementioned equations, a relaxation factor δ_p is adopted to stabilize the computations. It is defined by

$$\Xi_p^{(n)} = (1 - \delta_p)\, \Xi_p^{(n-1)} + \delta_p\, \Xi_p^{(n)*}, \tag{11}$$

where the superscripts (n) and $(n-1)$ indicate the values at the nth and $(n-1)$th iterations respectively, and the asterisk indicates the most recently corrected value. The relaxation parameter δ_p used is similar to that of Hennecke, Sparrow & Eckert (1971). The line iterative method is repeated until two successive iteration values of Ψ, Ω and T^* agree to within 0.1 %.

4. Results and discussions

4.1. *Flow patterns*

Typical photographs of flow patterns visualized under several surface temperatures T_h of the hot wall and inclination angles θ are shown in figures 5–9 together with those of the streamlines predicted. It may be seen from these figures that there is a similarity of the photographs of streaklines to the predicted flow patterns of streamlines.

Figures 5 (*a–c*) for $\theta = 60°$, 90° and 120° respectively show the flow pattern observed for $T_h = 4$ °C. These flows seem to be very stable and two-dimensional. One eddy in figures 5 (*a*) for $\theta = 60°$ circulates in the counterclockwise direction and spreads fully in the square cavity; that is, the movement of the eddy is upward along the cold wall and downward along the hot wall. The flow behaviours for $\theta = 90°$ and 120° as shown in figures 5 (*b*, *c*) are basically similar to that for $\theta = 60°$. However, as the inclination angle θ increases, the circulation rate of the eddy becomes larger and the flow vigour is increased since the water layer near 4 °C (its maximum density) occupies the vertical and upper part (top-heavy condition) in the cavity.

Figures 6 (*a–c*) for $\theta = 30°$, 90° and 150° respectively present the flow patterns for $T_h = 6$ °C. In figure 6 (*a*) for $\theta = 30°$, one eddy circulates slowly in the counterclockwise direction near the cold wall, and the other secondary eddy circulating clockwise appears near the hot wall. The appearance of two eddies in the water layer can be explained as follows. The cold water at 0 °C, which has a lower density than that at

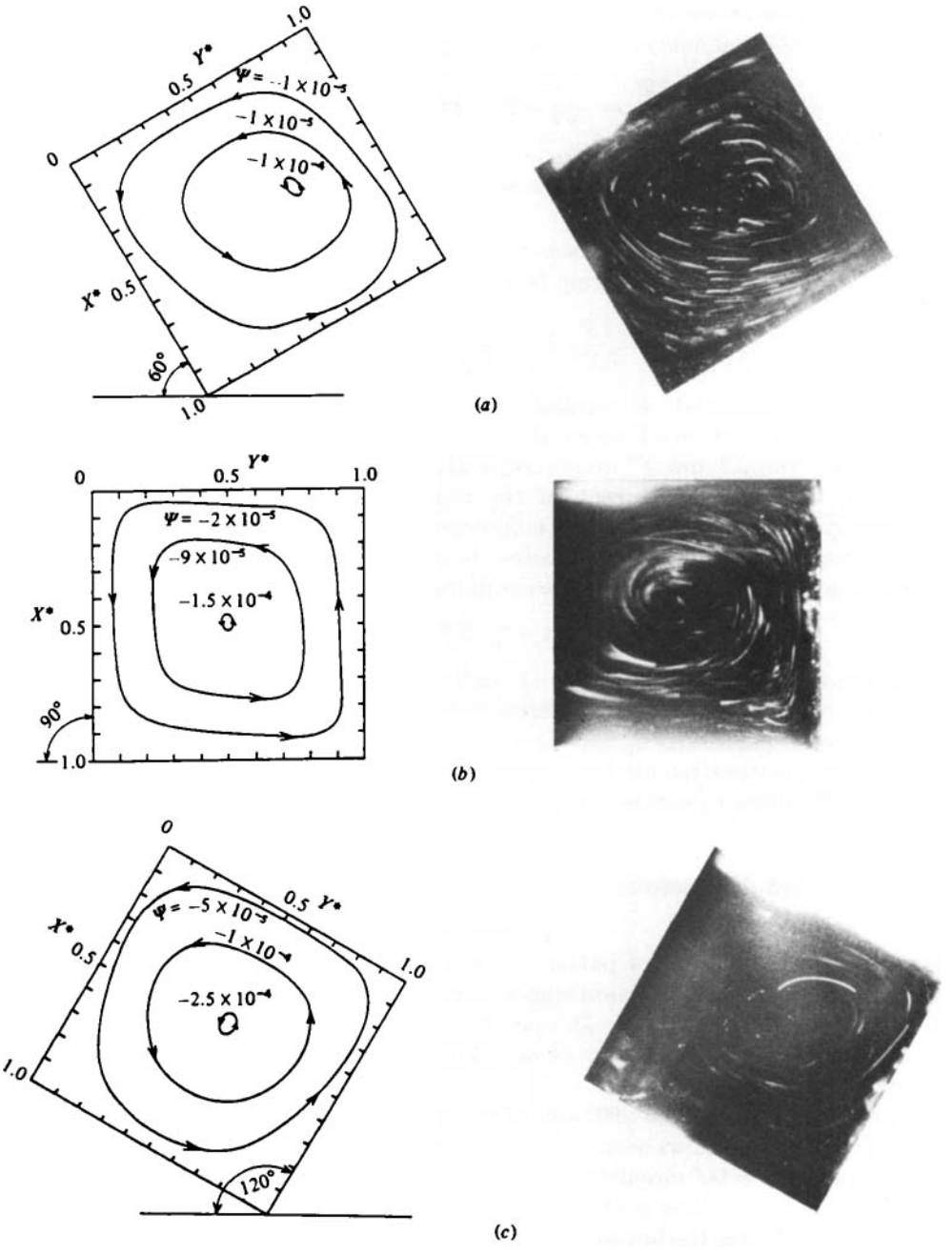

FIGURE 5. Flow patterns for $T_h = 4$ °C (solid lines predicted): (*a*) $\theta = 60°$; (*b*) 90°; (*c*) 120°.

about 4 or 6 °C, ascends along the sloping cold wall ($Y^* = 1$) and turns to the left on the upper wall ($X^* = 0$). On the other hand, the hot water at 6 °C, which has a lower density compared with that at about 4 °C, ascends along the sloping hot wall and collides withe the cold water descending from the cold wall ($Y^* = 1$). Consequently, two counter-rotating eddies appear in the water layer owing to the existence of a water layer having a maximum density at about 4 °C. As θ increases, the influence of the

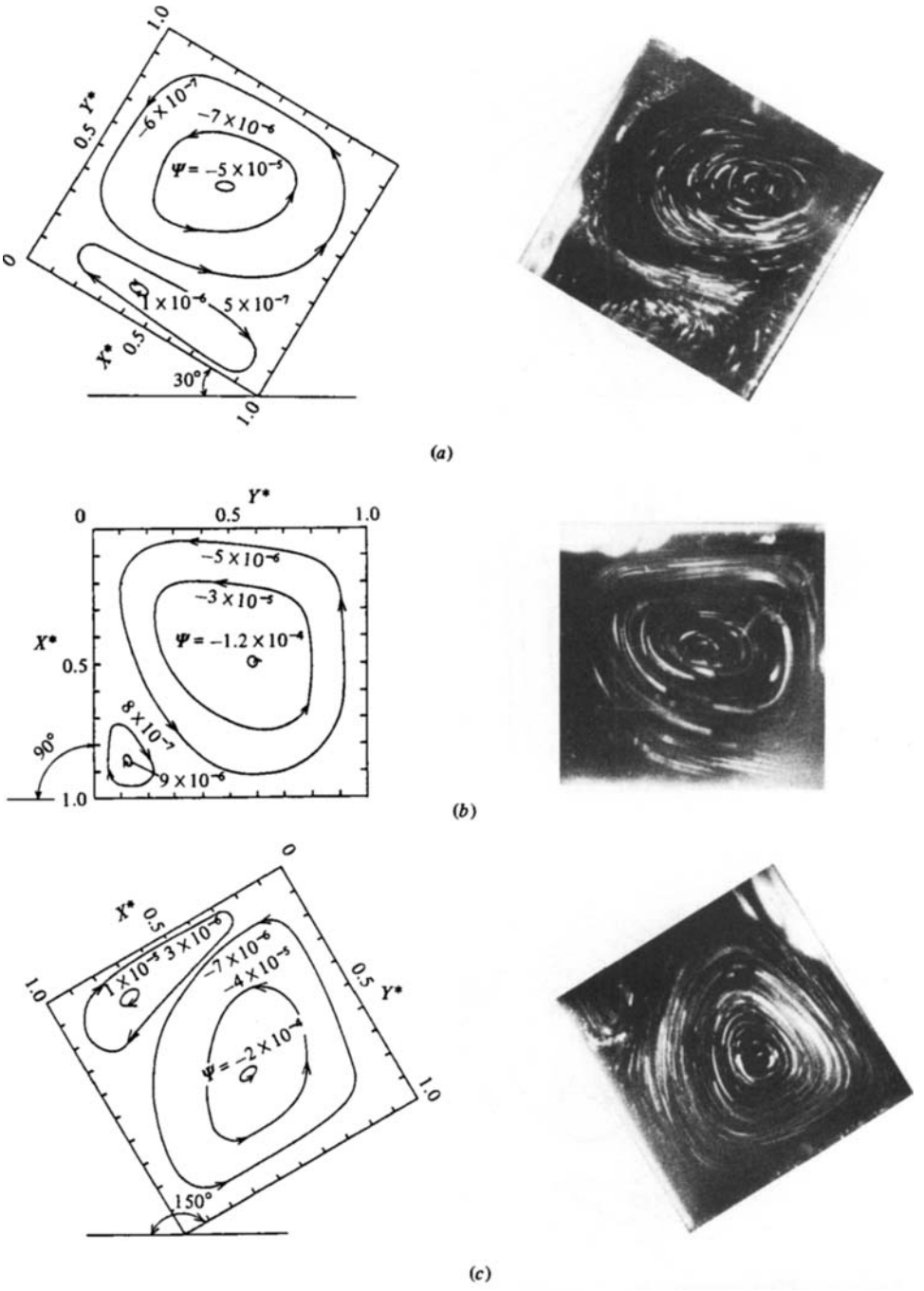

FIGURE 6. Flow patterns for $T_h = 6$ °C (solid lines predicted): (*a*) $\theta = 30°$; (*b*) 90°; (*c*) 150°.

counter-clockwise eddy near the cold wall is increased, while the counter-rotating secondary eddy is suppressed to the lower part of the hot wall.

Figures 7 (*a–c*) show various flow patterns for $T_h = 8$ °C and $\theta = 30°$, 90° and 150° respectively. In figure 7 (*a*) for $\theta = 30°$ one eddy circulating in the clockwise direction near the hot wall positioned at the lower part becomes influential, while the other,

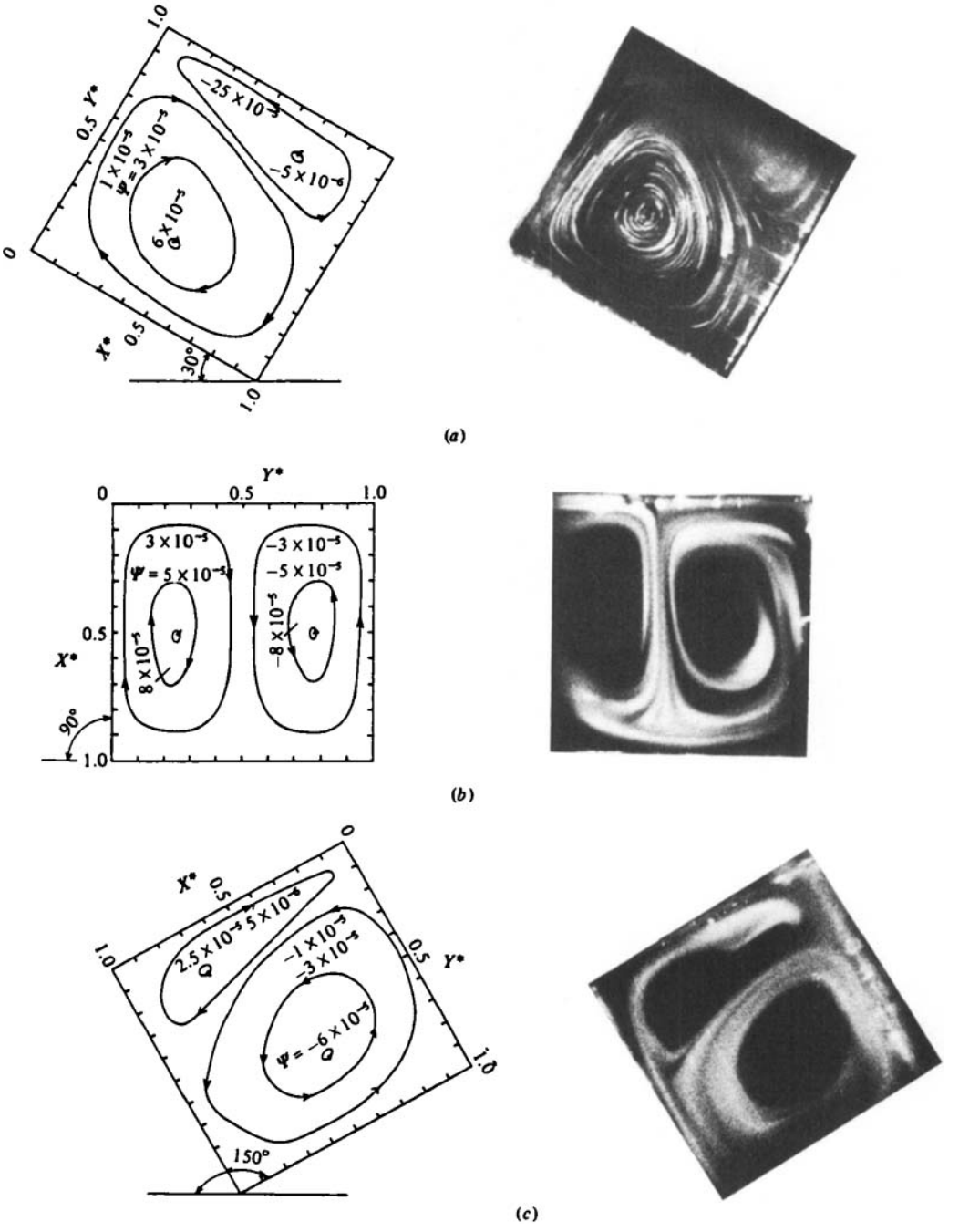

FIGURE 7. Flow patterns for $T_h = 8$ °C (solid lines predicted): (*a*) $\theta = 30°$; (*b*) 90°; (*c*) 150°.

weak, eddy circulating counterclockwise appears near the cold wall. For $\theta = 90°$ in figure 7(*b*) the effect of density inversion of water becomes more evident; that is, the eddy near the cold wall as seen in figure 7(*a*) becomes large, and finally two counter-rotating eddies of almost equal size emerge in the cavity since the density of water near the hot wall (8 °C) and cold wall (0 °C) becomes almost the same, as can be seen in figure 1. The almost-equal densities of water at 0 and 8 °C results in

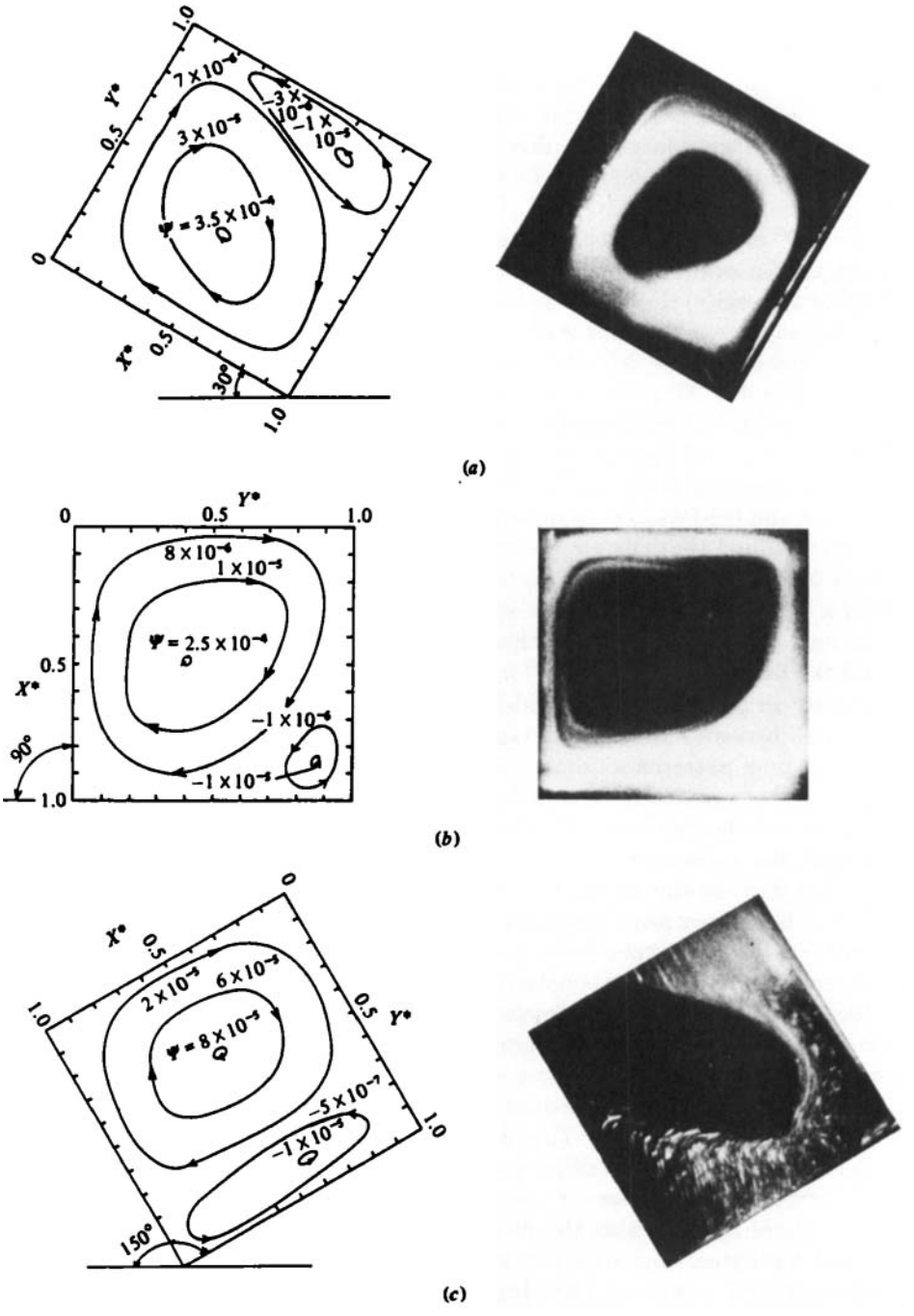

FIGURE 8. Flow patterns for T_h = 10 °C (solid lines predicted): (*a*) $\theta = 30°$; (*b*) 90°; (*c*) 150°.

an identical circulating speed of two counter-rotating eddies which ascend alongside each other up hot and cold walls and collide with each other at about $Y^* = 0.5$ near the upper wall ($X^* = 0$). For θ = 150 °C in figure 7(*c*) one eddy near the cold wall becomes influential and the other, counter-rotating eddy is suppressed to the hot wall in contrast with the eddies observed for $\theta = 30°$ in figure 7(*a*).

Figures 8(*a–c*) for $\theta = 30°$, 90° and 150° respectively present the flow patterns for

$T_h = 10$ °C. In figure 8(*a*) for $\theta = 30°$ the observed flow seems to be unstable and three-dimensional. That is, one eddy circulating clockwise appears in a whole part of the cavity. This anomalous unsteadiness of the flow pattern could result from the instability which appears in the transient flow behaviour at $\theta = 30°$ from the two-dimensional boundary-layer flow developed near the hot and cold walls observed at $\theta = 90°$ to a three-dimensional Bénard cellular-type flow (reported by Hart 1971; Krishnamurti 1970).

For $\theta = 90°$ in figure 8(*b*) the influence of one eddy near the hot wall is decreased and that of the other counter-rotating eddy near the cold wall is increased. For $\theta = 150°$ in figure 8(*c*) the observed flow seems to be very slow, and the fluid becomes almost stagnant near the cold wall.

Figures 9(*a–c*) for $\theta = 30°$, 90° and 150° respectively show the flow patterns for $T_h = 14$ °C. For $\theta = 30°$ in figure 9(*a*) one basic main boundary-layer flow circulating unstably and three-dimensionally in the clockwise direction appears at the inside of the surface walls, and two secondary eddies emerge in the centre core region owing to a viscous shearing force induced by the outside main boundary layer developed near the hot and cold walls as mentioned previously for a Boussinesq fluid. Therefore it can be explained that the appearance of these secondary eddies is independent of the effect of density inversion of water, since the density of water at 14 °C near the hot wall is smaller (99.94 % of that at 0 °C near the cold wall). For $\theta = 90°$ in figure 9(*b*) the flow pattern is similar to that for $\theta = 30°$. However, the circulating rate of flow and the flow vigour for $\theta = 90°$ is decreased as compared with those for $\theta = 30°$. For $\theta = 150°$ in figure 9 one weak eddy appears near the hot wall, and the fluid near the cold wall becomes almost stagnant.

For some flow patterns as shown in figures 5–9 there can be seen a difference of flow patterns between numerical and experimental results in the case of large surface temperature of the hot wall $T_h (\geqslant 8$ °C), the coexistence of two counter-rotating eddies, and the existence of a transition region from two-dimensional to three-dimensional flow as the inclination angle changes. For these natural convections caused by a buoyancy force based on temperature difference, a variation of thermal boundary condition in experiment would lead to a different flow behaviour from the flow pattern predicted under constant boundary condition by numerical analysis. In particular, as the surface temperature T_h of the hot wall is increased, the amount of heat transmitted by thermal conduction from the hot wall to the cold wall is increased through the lucite frame (10 mm thickness) consisting of the walls at $X^* = 0, 1$, and new temperature distributions on $X^* = 0, 1$, which are different from those predicted, are built up. This formation of new temperature distributions in experiments would cause the difference between numerical and experimental results for flow patterns in the case of coexistence of two weak counter-rotating eddies. Moreover, there appears also the disparity of flow patterns between experimental results and numerical ones based on the two-dimensional flow model in the range of inclination angle $\theta = 30°$ and 150°. It is presumed that these inclination angles would belong to the region of the transition of unstable flow from two-dimensional to three-dimensional or stagnant; in which region it may be impossible to apply the present two-dimensional model analytically.

4.2. *Temperature profiles of water layer*

Typical non-dimensional temperature distributions T^* of the water layer in the Y^* direction at the position $X^* = 0.5$ are shown in figures 10–12 for $\theta = 30°$, 90° and 150° respectively for various T_h. In these figures (*a*) shows the experimental results and

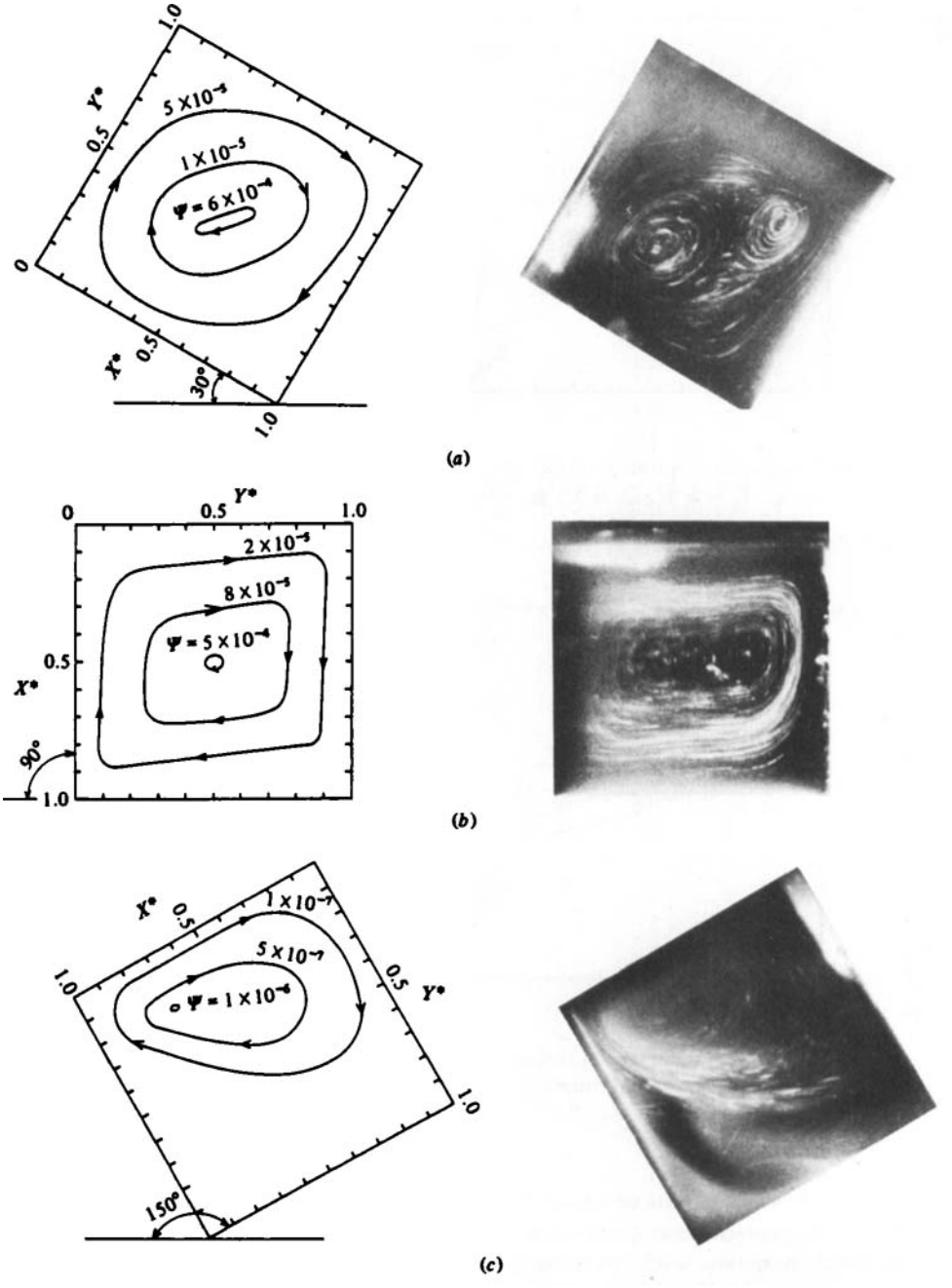

FIGURE 9. Flow patterns for $T_h = 14$ °C (solid lines predicted): (*a*) $\theta = 30°$; (*b*) 90°; (*c*) 150°.

(*b*) the predicted ones. Figure 10(*a*, *b*) for $\theta = 30°$ show the relationship between T^* and Y^* for various T_h. In these figures one can note that, as T_h increases, the temperature profile changes gradually from the almost-linear relationship between T^* and Y^*, which indicates the conductive heat transfer in case $T_h = 4$ °C, to the curved temperature profile (S-type), which indicates the natural convection in

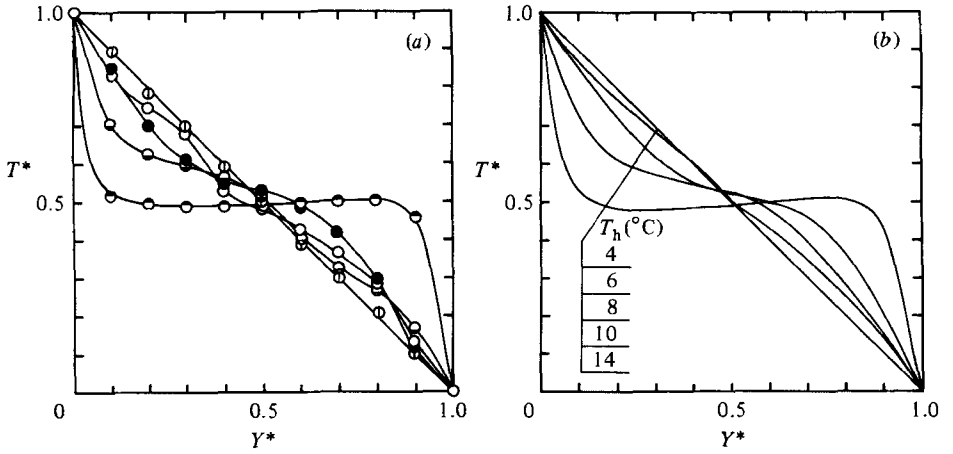

FIGURE 10. Temperature profiles in the Y^* direction for $\theta = 30°$ at $X^* = 0.5$. (*a*) Experimental results: ⦶, $T_h = 4$ °C; ○, 6 °C; ●, 8 °C; ◒, 10 °C; ◓, 14 °C. (*b*) Numerical results.

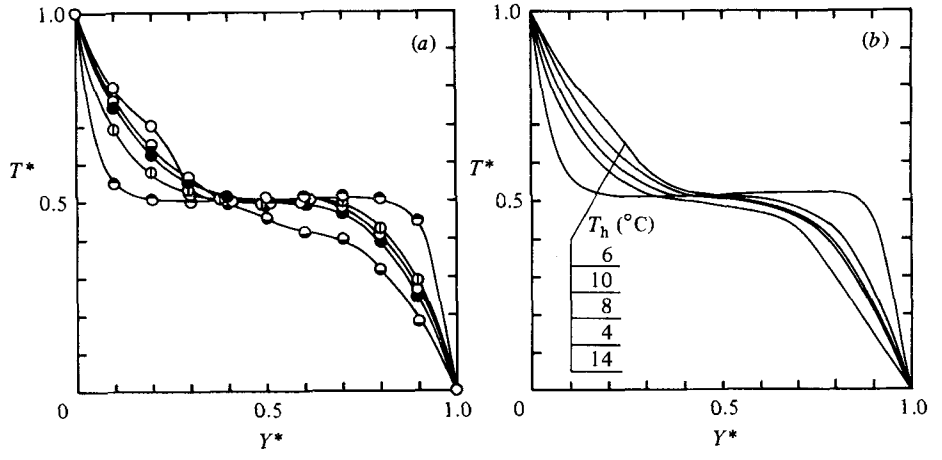

FIGURE 11. Temperature profiles in the Y^* direction for $\theta = 90°$ at $X^* = 0.5$: (*a*) experimental results; (*b*) numerical results.

case $T_h = 14$ °C. One can presume that, judging from an increase of the precipitous drop of temperature near the hot or cold wall with increasing T_h, the influence of the convection increases with increasing T_h. It is interesting to note that a steep drop of temperature for $T_h = 6$ °C appears in the range $Y^* = 0.4$–0.5. This steep drop of the fluid temperature would be caused by a collision between one fluid flow having a high temperature from the hot wall ($T_h = 6$ °C) and the other fluid flow having a low temperature from the cold wall ($T_h = 6$ °C) and the other fluid flow having a low temperature from the cold wall ($T_h = 0$ °C) as shown in the photograph of figure 6 (*a*). Temperature distributions of the water layer for $\theta = 90°$ are presented in figures 11 (*a*, *b*). The results of temperature distributions for $\theta = 90°$ at each T_h are similar basically to those for $\theta = 30°$, as can be seen in figure 10. However, one can note that a precipitous drop of temperature for $T_h = 6$ °C and $\theta = 30°$ moves to the hot wall

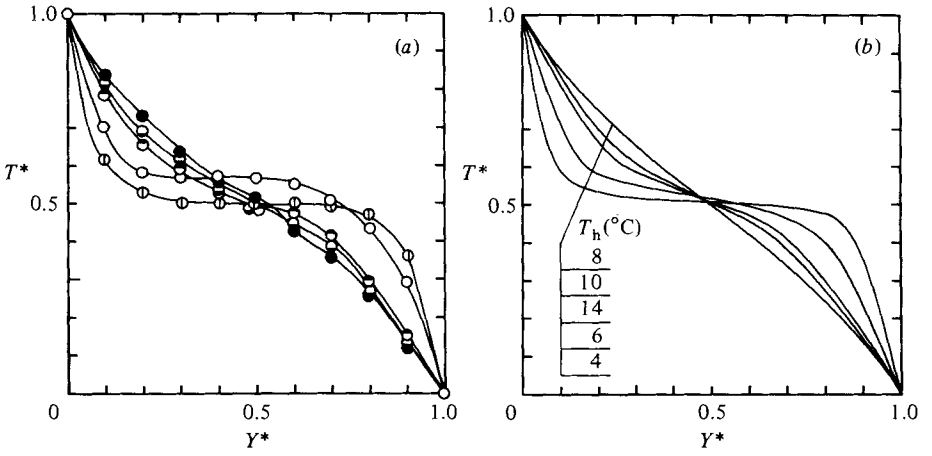

FIGURE 12. Temperature profiles in the Y^* direction for $\theta = 150°$ at $X^* = 0.5$: (a) experimental results; (b) numerical results.

in the range $Y^* = 0.2$–0.3 for $\theta = 90°$, and this temperature behaviour corresponds to the flow pattern for $\theta = 90°$, as can be observed in figure 6(a).

Figure 12(a, b) show the temperature distributions of the water layer for $\theta = 150°$. The results of temperature profiles for various T_h in the case $\theta = 150°$ are the inversion of those in the case $\theta = 30°$ as shown in figure 10. That is, from the temperature distribution in figure 12 it can be presumed that the mode of heat transfer through water layer is shifted gradually from convection to thermal conduction as θ increases for $T_h = 4$ °C. In comparison between experimental and numerical results for the temperature, the difference between them may be explained as being due to incomplete insulation at the walls ($X^* = 0.1$) in experiments and the previously mentioned disparity of flow patterns in experiment and analytical model for some inclination angle. From these experimental and numerical results for the temperature distributions of the water layer, one can note that the temperature distributions measured show a similar tendency to those predicted.

4.3. *A comparison of natural-convection heat transfer between the present data and the previous data using Boussinesq fluids*

A comparison of natural-convection heat transfer in an inclined rectangular cavity between the present data and those obtained by previous investigators (Buchberg, Catton & Edwards; O'Toole & Silveston 1961) is shown in figure 13. They summarized their experimental results for Boussinesq fluids without density inversion in the range of $\theta \leqslant 60°$, and presented their correlations in terms of average Nusselt number $Nu = qW/\lambda\,\Delta T$ and Rayleigh number $Ra\cos\theta = g|\beta|TW^3\cos\theta/\nu\alpha$, where β is the thermal expansion coefficient, α the thermal diffusivity and g the gravitational acceleration. The physical properties of the fluid used were evaluated at the average temperature of the hold and cold walls. However, the effect of density inversion on the convective heat transfer was not discussed in their studies. In figure 13 the present data for $\theta = 120°$–$180°$ in the range $T_h \leqslant 6$ °C and for $\theta = 0°$–$60°$ in the range $T_h \geqslant 10$ °C are plotted according to the previous method, considering the above-mentioned flow patterns and the temperature distributions. The present data agree well with those of previous investigators in the temperature ranges without the effect of density inversion; that is, $T_h \leqslant 4$ °C and $T_h \geqslant 14$ °C. However, it can be seen that

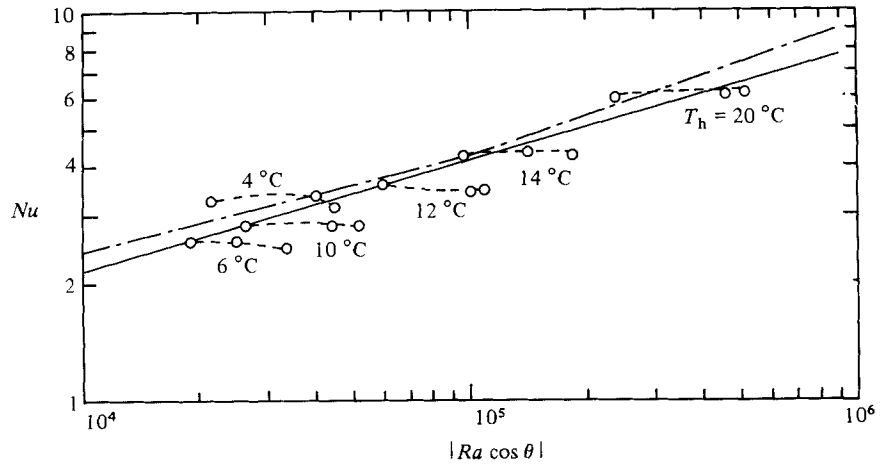

FIGURE 13. A comparison of the average Nusselt number Nu between the present data and previous ones: ○, present data, T_h = 0–6 °C for θ = 120°–180°, T_h = 10–20 °C for θ = 0°–60°; ——, results of Buchberg *et al.*, $Nu = 0.104\ (Ra \cos\theta)^{0.285}$ (without density inversion); —·—, O'Toole & Silvestone's results (without density inversion).

the present data resulting from the strong effect of density inversion of water in the range T_h = 6–12 °C lie below the previous results. These differences can be explained by the fact that convective heat transfer through the water layer is prevented by two counter-rotating eddies due to the density inversion of water near 4 °C, as shown in photographs of the flow patterns in figures 6–8.

4.4. *The influence of inclination angle θ on the average Nusselt number Nu*

Figure 14 presents the relationship between Nu and θ for various T_h, which are obtained by experiments and numerical analyses (solid lines), together with Tien's (1968) data. In this figure it can be seen that the value of Nu changes in a complicated manner with increasing θ depending on T_h. For $T_h < 8$ °C Nu increases gradually with increasing θ, and it reaches a maximum value between $\theta = 120°$ and 150°. Moreover, in the range $\theta < 90°$ Nu becomes smaller, since the influence of convection is reduced by the existence of a lighter water layer at 0 °C in the upper part in the water layer. In contrast, in the range $\theta > 90°$ the value of Nu becomes large, since convection becomes influential owing to the existence of a top-heavy fluid layer as shown in figures 5(*c*) and 6(*c*). In case $T_h = 8$ °C it can be seen that Nu increases gradually with increasing θ from 0° to 90°, and reaches a maximum value at about $\theta = 90°$, while Nu decreases gradually with increasing θ from 90°. On the other hand, for $T_h > 8$ °C, the change of Nu against θ indicates the reverse tendency as compared with that for $T_h < 8$ °C. That is, Nu increases slightly with increasing θ for $\theta < 60°$, it reaches a maximum at about 60°, and for $\theta > 60°$ Nu decreases steeply with increasing θ. This behaviour of Nu against θ is similar to previous results obtained by using a Boussinesq fluid without density inversion. By comparison between the experimental and numerical results, the numerical results of Nu shows good agreement with the experimental ones in the range $T_h < 8$ °C ($0° \leqslant \theta \leqslant 120°$), $T_h > 8$ °C ($30° < \theta \leqslant 180°$) and $T_h = 8$ °C ($0° \leqslant \theta \leqslant 180°$). However, the difference in Nu between both results exists in the case $T_h < 8$ °C ($150° \leqslant \theta \leqslant 180°$) and $T_h > 8$ °C ($0° \leqslant \theta \leqslant 30°$), because of the difference of flow patterns between experiment and analysis, as can be observed in figures 8(*a*) and 9(*a*).

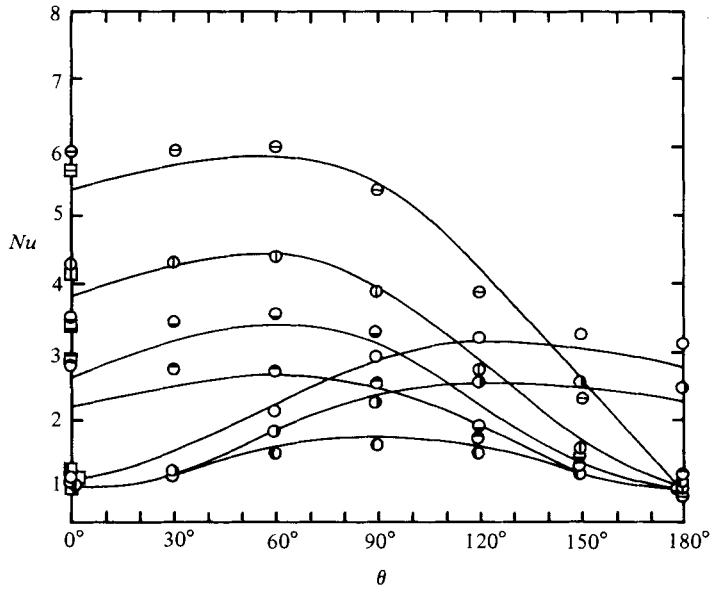

FIGURE 14. Relationship between average Nusselt number Nu and inclination angle θ. Present data: ○, T_h = 4 °C; ◑, 6 °C; ◐, 8 °C; ◓, 10 °C; ◒, 12 °C, ⓘ, 14 °C; ⊖, 20 °C. ——, prediction. □, Tien's data ($\theta = 0°$).

4.5. *The effect of temperature T_h of the hot wall on the average Nusselt number Nu*

Figure 15 shows the relationship between Nu and T_h ($= \Delta T$) for various values of θ obtained by experiments and numerical analyses (solid lines). In this figure it is evident that Nu does not increase monotonically with increasing T_h as in the case of a Boussinesq fluid without density inversion. Namely, for $T_h \leqslant 4$ °C, when a single eddy occupies the entire part of the fluid layer, as T_h becomes higher, Nu increases monotonically till it reaches a peak point at about 4 °C because the flow vigour is increased with increasing density difference of water in the cavity. But the minimum value of Nu appears at about 8 °C. The appearance of such a minimum value of Nu at about 8 °C may be caused by the existence of two counter-rotating eddies as shown in figure 7, where heat exchange by convection from the hot wall to the cold wall is performed by a collision between two counter-rotating eddies and the decrease of the flow vigour of two counter-rotating eddies due to a collision between them. That is, it takes a longer distance for two counter-rotating eddies to transfer the heat from the hot wall to the cold wall, and their circulation rates are decreased, as compared with that of a single eddy without density inversion. And Nu increases monotonically again with increasing T_h in the range $T_h > 8$ °C. This increase of Nu could be explained from the fact that the flow vigour near the hot wall increases with increasing T_h since the density of water at $T_h > 8$ °C becomes smaller than that at 0 °C and it decreases almost linearly with increasing T_h. This peculiar relation between Nu and T_h appears in the range $\theta = 60°$–$150°$. However, the variation of Nu with T_h for $\theta = 0°$–$30°$ and 180° is different from that for $\theta = 60°$–$150°$. In the case $\theta = 0°$–$30°$ Nu increases gradually with increasing T_h for $T_h \leqslant 8$ °C, and it increases steeply with T_h in the range of $T_h > 8$ °C. That is, the influence of convection becomes remarkable for $T_h > 8$ °C. On the other hand, in the case $\theta = 180°$ the change of Nu with T_h for $T_h \leqslant 8$ °C is similar to that for $\theta = 60 - 150$ °C, but for $T_h > 8$ °C Nu decreases gradually with

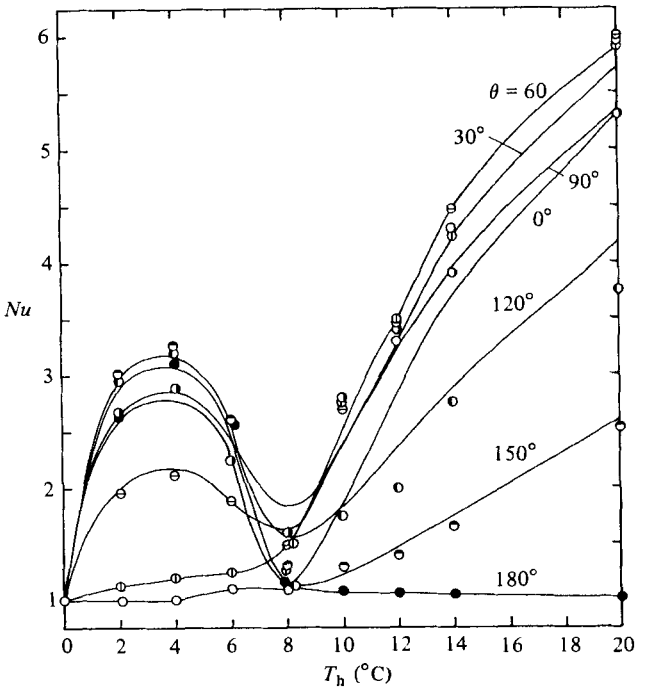

FIGURE 15. Relationship between average Nusselt number Nu and surface temperature T_h of the hot wall. Present data: ○, $\theta = 0°$; ⊕, 30°; ⊖, 60°; ◑, 90°; ◐, 120°; ◓, 150°; ●, 180°. ——, Prediction.

increasing T_h, and also the absolute value of Nu becomes small. The difference between experimental and numerical results for Nu for some ranges of θ and T_h can be explained from the reasons in §4.4.

5. Conclusions

The behaviour of natural-convection flows with the effect of density inversion of water in an inclined square cavity, with one hot wall kept at various uniform temperatures and the opposing cold wall maintained at 0 °C, has been clarified by experiments and numerical analyses based on an assumption of two-dimensional laminar flow. From the aforementioned results it can be concluded that the flow patterns of water in the cavity are changed by the effect of density inversion and inclination angle of the cavity; consequently the density inversion and inclination angle have an important effect on natural convection in the inclined square cavity. It is clear that two counter-rotating eddies due to the density inversion disturb the convective heat transfer from the hot wall to the cold wall, and the influence of two counter-rotating eddies is strongly dependent on the inclination angle. It can be claimed that the present numerical results agree well with the experimental ones for some regions of inclination angle and surface temperature of the hot wall.

The authors would like to thank Prof. Nobuhiro Seki and Associate Prof. Shoichiro Fukusako, Faculty of Engineering, Hokkaido University, for their encouragement and helpful suggestions throughout this work.

REFERENCES

BUCHBERG, H., CATTON, I. & EDWARDS, D. K. 1976 *Trans. ASME* C: *J. Heat Transfer* **98**, 182.

CLEVER, R. M. & BUSSE, F. H. 1977 *J. Fluid Mech.* **81**, 107.

DEGRAAF, J. G. A. & VAN DER HELD, E. F. M. 1953 *Appl. Sci. Res.* **3**, 393.

HART, J. E. 1971 *J. Fluid Mech.* **47**, 547.

HENNECKE, D. K., SPARROW, E. M. & ECKERT, E. R. G. 1971 *Wärme- und Stoffübertragung* **4**, 222.

KRISHNAMARTI, R. 1970 *J. Fluid Mech.* **42**, 295.

LINTHORST, S. J. M., SCHINKEL, W. M. M. & HOOGENOORN, C. J. 1981 *Trans. ASME* C: *J. Heat Transfer* **103**, 535.

MERKER, G. P. & STRAUB, J. 1982 *Wärme- und Stoffübertragung* **16**, 63.

O'TOOLE, J. L. & SILVESTON, D. L. 1961 *Chem. Engng Prog. Symp. Ser.* **57**, 81.

OZOE, H. SAYAMA, H. & CHURCHILL S. 1977 *Intl J. Heat Mass Transfer* **20**, 123.

RUTH, D. W., RAITHBY, G. D. & HOLLANDS, K. G. T. 1980 *J. Fluid Mech.* **96**, 481.

SEKI, N., FUKUSAKO, S. & INABA, H. 1978 *Wärme- und Stoffübertragung* **11**, 145.

SUGAWARA, M., FUKUSAKO, S. & SEKI, N. 1974 *Trans. JSME* **40**, 3155.

SUN, Z. S., TIEN, C. & YEN, Y. C. 1969 *AIChE J.* **15**, 910.

TIEN, C. 1968 *AIChE J.* **14**, 652.

WATSON, A. 1972 *Q. J. Mech. Appl. Maths* **15**, 423.